2020 IEEE/RSJ International Conference on Intelligent Robots and Systems (IROS)
October 25-29, 2020, Las Vegas, NV, USA (Virtual)

Resonating Magnetic Manipulation for 3D Path-Following and Blood Clot Removal Using a Rotating Swimmer

Julien Leclerc[1], Yitong Lu[1], Aaron T. Becker[1], Mohamad Ghosn[2], and Dipan J. Shah[2]

***Abstract*— There are many design trade-offs when building a magnetic manipulator to control millimeter-scale rotating magnetic swimmers for surgical applications.**

For example, increasing the magnitude of the flux density generated by the magnetic manipulator increases the torque applied to the swimmer, which could enable performing a wider variety of surgical tasks in the future. However, producing stronger magnetic fields has drawbacks, such as increased active power usage.

To produce a quickly rotating field, EMs must be quickly charged and discharged. This results in a low power factor (high reactive power used in comparison with the active power). Adding capacitors in series with the electromagnets improves the power factor because the capacitors can provide reactive power. With this method, larger flux densities can be produced without necessitating an increase of the apparent power delivered by the power supplies.

This paper highlights the benefits of using capacitors for the magnetic manipulation of rotating swimmers. Rotating swimmers can be used to remove blood clots. The clot removal rate of resonating magnetic manipulators is measured using a realistic blood clot model. This paper also presents a control method for the currents inside the electromagnets that enable 3D navigation without current sensing.

I. Introduction

Rotating magnetic swimmers are small screw-shaped (or helical-shaped) devices that contain a permanent magnet (see Fig. 1). When they are subjected to a rotating magnetic field, they rotate. This rotational movement combined with the helical shape produces a propulsive force [1]–[8]. These devices can be propelled and steered in 3D [9]–[16] and could potentially navigate within the bloodstream of a patient to reach a pulmonary embolus [17]. Once there, the rotational movement could also be used to abrade the obstruction [18]–[24].

A. Case study: acute pulmonary embolism

Acute pulmonary embolism (PE), if left untreated, is a life-threatening disorder associated with high mortality rates worldwide. In the United States alone, about 300,000 individuals die from an acute PE every year [25]. An acute PE occurs when a thrombus dislodges from its site of origin (usually deep veins in the lower extremities). The thrombus then migrates as an embolus through the vena cava and the right side of the heart to the pulmonary arteries. Obstruction to pulmonary blood flow results in increased pulmonary pressure and afterload on the right ventricle (RV), leading to RV dilation and can result in a reduction in the forward stroke volume ejected by the RV. As a consequence, massive right heart failure may occur causing death from arrhythmia, hemodynamic collapse, and shock [26]–[28].

The severity of PE depends on the size and location of the emboli. Less severe PE (or submassive PE) can be minimally asymptomatic, while massive PE can be life-threatening. Rapid recognition and timely treatment are vital

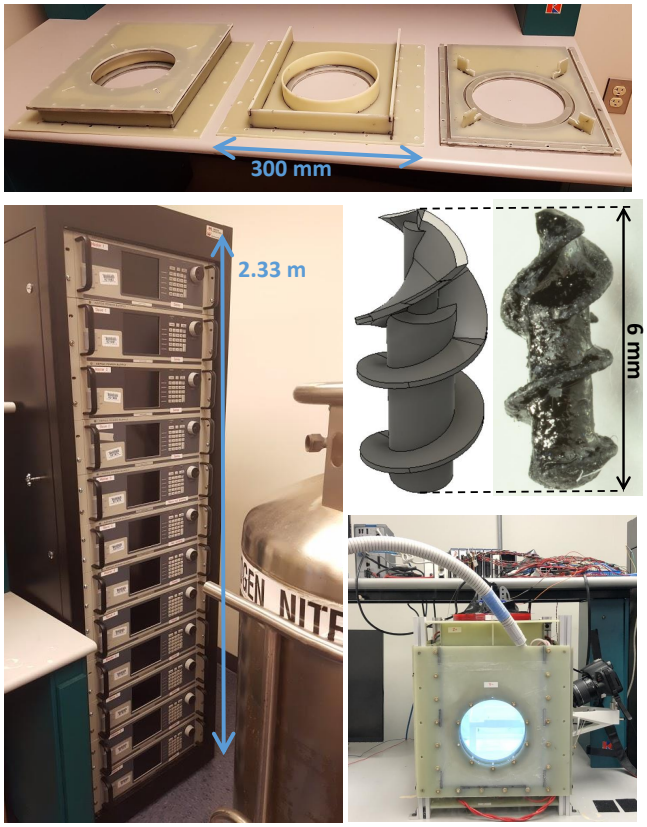

Fig. 1. Top: Photo of a cryostat of the magnetic manipulator. Bottom left: Photo of the power supplies rack. The tank of LN2 can be seen on the right side of this picture. Middle right: CAD model and photo of the swimmer. Bottom right: Photo of the magnetic manipulator when cooled by LN2. More details about this system can be found in [29].

*This work was supported by the National Science Foundation under Grant No. [1646607].

*Dr. Shah receives salary support from the National Science Foundation (grants CNS-1646566 and CNS-1931884) and the National Institutes of Health (1R01HL137763-01)

(1) Department of Electrical Engineering, University of Houston, 4800 Calhoun Rd, Houston, TX 77004, USA

(2) Houston Methodist DeBakey Heart & Vascular Center, 6550 Fannin Street, Houston, TX 77030, USA

jleclerc@central.uh.edu, ylu36@uh.edu, atbecker@central.uh.edu, mghosn@houstonmethodist.org, djshah@houstonmethodist.org

for successful outcomes. Approximately 10% of patients presenting with PE do not survive the acute episode [30]. Prompt diagnosis and treatment initiation can decrease the mortality rate to less than 10% [31].

In patients with low-risk or submassive PE, anticoagulant treatment is a first-line which is encouraged to be initiated even if the diagnostic work-up is ongoing. For patients with massive PE, systemic administration of thrombolytic therapy is considered lifesaving but has a potential for circulatory collapse (including hemorrhagic stroke) in 0.5 to 1.14% of cases [32]. Such patients are a good candidate for surgical embolectomy. Pulmonary artery catheterization to locally deliver thrombolytic medication has been used to improve outcomes for acute submassive PE [33]. An ultrasound transducer placed at the tip of the catheter is sometimes used to speed up thrombolysis (ultrasound-accelerated catheter-directed thrombolysis). The thrombus can also be removed using an aspiration tool with the catheter (aspiration thrombectomy). This procedure requires the availability of interventional procedural suites and skilled interventionalist physicians; this is routinely not available at small community-based hospitals where most of these patients initially present. The ability of more widespread emergent thrombolysis without incurring the bleeding risks of pharmacologic thrombolytic therapy is highly desirable. Rotating magnetic swimmers could allow safer thrombolysis as they can mechanically abrade blood clots and reduce the need for pharmacologic thrombolytic therapy.

Rotating swimmers typically rotate at frequencies in the range of 10 to 100Hz. A high rotational speed is desirable as it increases both velocity of the swimmer during navigation and blood clot removal rate (see Section III-B). An increase in removal rate is beneficial as it would allow a more rapid reperfusion and improve patient's outcome. The magnetic field can be generated by rotating permanent magnets or via non-moving electromagnets (EMs). The first solution requires heavy rotating parts that need to change speed continuously and quickly. This requires expensive, powerful electric motors. Also, heavy parts rotating and changing speed generate a moving obstacle in the operating room.

B. Powering a magnetic manipulator

The magnetic field produced by an EM is proportional to the current that circulates in it. The field produced by EMs can therefore be controlled by changing the voltage that is applied to it. Two EMs oriented along different axes are enough to create a rotating field by applying sinusoidal currents with a phase shift. Additional EMs enable producing fields that are more homogeneous and/or oriented in any direction.

EMs are made of a conductive wire wound into a coil. They are inductive loads and, as a result, consume a positive reactive power when subjected to an AC current. Power supplies need to be sized to provide the apparent power used by the loads. The *apparent power* is the sum of active and reactive power, so a circuit having a low power factor (high reactive power used in proportion to the active power) will result in large power supplies. Capacitors are components that consume negative reactive power and can be employed to compensate the reactive power used by the EMs. High power capacitors are commercially available in a wide range of values and are cheap ($12 USD for each of the 440/370 VAC, 30μF capacitors used in this study). When mounted in series with the EM, they form a resonating RLC circuit.

The use of capacitors would decrease the cost of clinical magnetic manipulators by decreasing the power rating needed for the power supplies. *Power rating* is a term that describes the maximum power of an equipment under normal use conditions. The set of power supplies is the most expensive component of the magnetic system used in this study. The cost of health care has increased significantly over the past few years. The price of medical imaging is a key contributor to US health care costs [34]. Therefore, it is important to reduce the price of medical equipment to provide quality care and cut costs. The concept of resonating magnetic manipulation was introduced by Nam et al. [35]. In that paper, the authors used a Helmholtz coil system together with capacitors. They used multiple sets of capacitors that could be dynamically connected and disconnected from the circuit. This method allows their system to be dynamically-tuned and therefore efficient within a broad range of frequencies. They demonstrated that using capacitors increased the robot swimming speed and the removal rate on blood clot models made of agar.

More work is needed to build a practical resonating magnetic manipulator. Current-regulated power supplies are often used to control the value of the current circulating inside EMs. They are typically made of two nested control loops, the internal one for current regulation and the external one for voltage regulation [36]. Voltage regulation is needed because the voltage of electrical networks can vary widely ($\pm$5% is allowed in the USA). Commercial current-regulated power supplies, however, have limited tuning parameters, and the performance of the regulation is often reduced with complex loads. A magnetic manipulator is a complex load because the circuit impedance changes with the frequency and the EMs are in magnetic interaction, and so induce voltages between each other. Two types of current sensing methods are available to perform current regulation. The first method is to measure the voltage across a shunt resistor, a component which has the disadvantage of introducing a voltage drop in the circuit and dissipating power. The second method relies on a magnetic measurement, by using either a Hall effect probe for AC+DC measurements or a copper coil for DC only acquisitions. Both are sensitive to electromagnetic noise and can suffer measurement errors in the presence of an external magnetic field. A sensorless current control method would solve these issues and offer the additional advantage of being more robust by removing the need for current control loops and the associated sensors. The robustness of the robotic surgical system is critical as a failure could cause the patient's death.

The present paper investigates the benefits of adding capacitors to a resonating magnetic manipulator. It also

introduces new tools and methods that allow closed-loop 3D path following without the need for current-mode power supplies. The experimental setup and the protocols used in this study are first described in Section II-A. This paper's main contributions are detailed into Sections III and IV; both focus on the use of resonating magnetic manipulators for the actuation of rotating swimmers. Section III investigates the frequency response of this type of system. It highlights theoretically and experimentally the benefits of adding capacitors. This section also shows, in III-A, that the electrical resistance of the EMs limits the current at the resonating frequency. It is experimentally shown in this section that the use of liquid nitrogen (LN2) allows decreasing the resistance of the EMs and allows generating stronger magnetic fields. In Subsection III-B, the removal rate of a helical swimmer is measured as a function of the rotational frequency of the magnetic field, with and without capacitors. A blood clot model made of real human blood and kept at body temperature is used. Section IV investigates the closed-loop 3D path-following of rotating swimmers using resonating manipulators. It introduces in Subsections IV-A to IV-C a new software module, called the Electric Model and Solver Module (EMSM), that computes the voltage to apply to the electric circuit to produce the desired current. The magnetic field magnitude and orientation are controlled via the current that circulates inside the EMs. A new open-loop current controller that uses the EMSM is experimentally compared to a regular current mode power supply in Subsections IV-E performing closed-loop 3D path-following. Section V is a conclusion about this work and the potential benefits that capacitors could have when used for clinical magnetic manipulation.

II. Experimental Setup and Protocols

A. Hardware description

The magnetic manipulator used in this study was extensively presented in [29] and is only briefly described here. Some components of the system are shown in Fig. 1. The system is made with six EMs arranged in a cube shape. The EMs have internal and external radii of 180mm and 215mm, respectively, and separated by a distance of 300mm. They are placed inside cryostats that can be filled with liquid nitrogen to improve their cooling and decrease their resistance. The workspace is thermally insulated via styrofoam, and its internal walls encapsulate a resistive heating element. A thermocouple measures the temperature of the air inside the workspace, which can be regulated. Each EM is powered by a set of two Kepco BOP 20-50MG power supplies connected in series. Each set can provide up 2kW of power under a maximum voltage of 100V. They can either work in voltage or current mode. The power supplies are controlled via an external analog signal generated by an industrial controller (National Instrument IC3173). Two Basler acA800 cameras are used to measure the position of the swimmer during the 3D path-following. The industrial controller performs image processing and other real-time computation. Six capacitors (each 30μF) were added to compensate for the reactive power

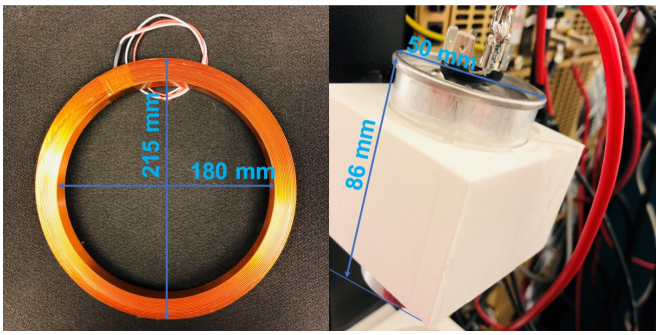

Fig. 2. Picture of an EM (left) and of a capacitor (right) used in this study.

used by EMs. Custom supports to hold the capacitors on the back of the power supplies were designed and built (see Fig. 2). The capacitors are connected in series with the EMs.

A 3D drawing of the swimmer used for clot removal and 3D path-following is shown in Fig. 1. The swimmer is screw-shaped with a pitch and diameter of 2.5mm. The length of the swimmer is 6mm. This size was chosen because it is small enough to be inserted inside an artery and large enough to be easily manufactured. This size also allows efficient swimming and a high blood clot removal rate. The body was 3D printed using a Projet 3510 HD. This fabrication method produces a swimmer that does not have sharp edges. A NdFeB permanent magnet having a length of 1mm and diameter of 0.75mm is placed inside the 3D printed body and glued with epoxy. The tip of the swimmer is coated with diamond powder (grain size 106–125μm) to promote abrasion. The coating was made by first dipping the tip of the swimmer in epoxy and and then sprinkling diamond powder onto it.

1) Blood clot preparation: The presented study involves human volunteers and was reviewed and approved by an IRB. Blood was taken from a healthy volunteer using a sterile lancet and dispensed onto a Petri dish. A pipet was used to measure 50μL of blood and place it inside a cylindrical channel made with PDMS (see Fig. 3). The channel represents a blood vessel and has a diameter of 3mm and length of 30mm. The channel with blood was then placed into the magnetic manipulator, and left inside for 55 minutes for the blood clot to form. The temperature inside the magnetic manipulator was regulated to human body temperature (37°C). A temperature sensor is present inside the magnetic manipulator, as well as a heating element. A temperature regulator was programmed using LabVIEW. After waiting 55 minutes, phosphate-buffered saline (PBS) solution was added inside the channels to fill them, a process that takes approximately 5 minutes. PBS is a water-based salt solution that has the same pH as human blood.

2) Clot removal protocol: The swimmer was first inserted into the channel. The channel was then placed into the magnetic manipulator which is still heated to human body temperature. A Canon EOS RebelSL2 camera was placed on the top of the magnetic manipulator to monitor the swimmer.

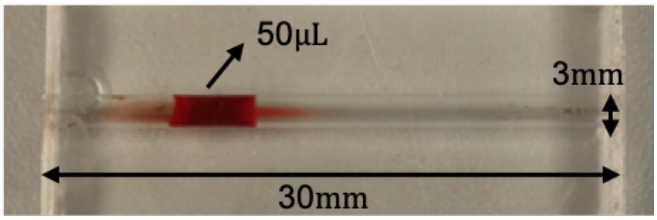

Fig. 3. Picture of an blood clot made inside a PDMS channel. The channel has a diameter of 3mm.

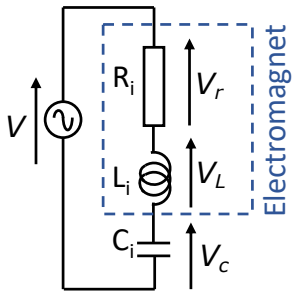

Fig. 4. Schematic presenting the variable names used for the current and voltages in a resonating circuit.

The experimental process was monitored in real time through a display screen. The removal time taken by the swimmer to remove each blood clot was measured from the recorded video. The removal rate was calculated by dividing the initial clot volume (50μL) by the removal time. If a swimmer failed to completely remove the blood clot during the experiments, no removal rate was calculated. Multiple sets of comparative experiments were done with and without capacitors and for different frequencies. The peak value of the voltage applied to the EMs was the same for all clot removal experiments and equal to 100V. After the experiments, the material in contact with blood was soaked and washed in bleach to prevent potential contamination.

B. Blood rheology mimicking solution

The liquid used for 3D path-following in Subsection IV-E is similar to the one used in [17]. It is a made of 27.5% glycerol and 10% ethyl alcohol mixed with water. The viscosity and density of this liquid were measured and are 3.10^{-3} Pa·s^{-1} and 1.05g/mL respectively, values that are within the normal range for human blood [37], [38].

III. Frequency Response

In this paper j represents the complex operator i.e. $j^2 = -1$. Variables which have their name written in a bold font and uppercase letters are matrices. Variables which have their name written in a bold font and lowercase letters are vectors. Non-bold variables are scalars.

A. Circuit impedance

The calculation of the frequency response of an RL or RLC circuit is trivial using complex numbers. It is necessary for the sizing of the capacitor and helps to understand the functioning of the system. The frequency response calculated in this subsection does not take into account the magnetic interaction between electromagnets. This interaction is taken into account in Subsection IV-A.

The complex impedance Z_l for an inductance L is $Z_l = j \cdot L \cdot \omega$ where ω is angular frequency in rad/s. The complex impedance Z_c for a capacitance C is $Z_c = 1/(j \cdot C \cdot \omega)$. The equation that links complex current I and voltage V inside an electric circuit is $V = Z \cdot I$ where Z is the complex impedance of the load. For an RLC circuit (shown in Fig. 4), the impedance is equal to $Z = R + j(L \cdot \omega - \frac{1}{C \cdot \omega})$. The resonating frequency $f_0 = \frac{1}{2\pi\sqrt{L \cdot C}}$ is the minimum norm of Z. At resonating frequency, the value of current is maximum and equal to V/R. Lowering the resistance of the EM increases the maximum current value, provided that it does not exceed the power supplies' capability. Reducing the electrical resistance of EMs can be accomplished by using a wire with larger diameter (which would require adding a few more turns in the winding to achieve the same inductance) or by cooling the winding to low temperature using liquid nitrogen, see [29].

It was previously demonstrated that the swimmer used in this study could remove blood clots at rotating frequencies of up to 55Hz without capacitors. It was expected that capacitors would increase this value, and therefore 30μF capacitors were selected. These capacitors in series with the EMs generate a resonating frequency of 65Hz, which represents an increase of 15% of the rotational speed. The current inside an EM is plotted in Fig. 5 as a function of the frequency for a constant input voltage amplitude of 100V. Measurements were also performed with a capacitor value of 15μF and results show that theoretical values are consistent with the measurements. Tests were made with the EM passively cooled and with the EM cooled by immersing in LN2.

Cooling with LN2 allowed experimentally reaching a current value of 21.8A, while with passive cooling the maximum current is 3.6A. The RLC circuit only exhibits relatively high current in a limited frequency band. Below 45Hz, using a circuit without a capacitor is more efficient. A solution to this issue is proposed in [35], where the authors use a system to dynamically connect and disconnect capacitors to tune the system to the working frequency.

B. Blood clot removal

1) Blood clot removal: The blood clot removal rate was measured as a function of the magnetic field rotational frequency. The peak value of the voltage applied to the circuit was 100V for all tests. Fig. 6 compares the removal rate obtained with and without capacitors in the circuit.

The blood clot applies a torque on the swimmer that increases with the rotational speed. The maximum torque is reached when the magnetic moment of the swimmer is perpendicular to the applied field. The rotational frequency that produces a torque on the swimmer equal to the maximum torque is called the *step-out frequency* f_{so}. For $f_{mf} < f_{so}$

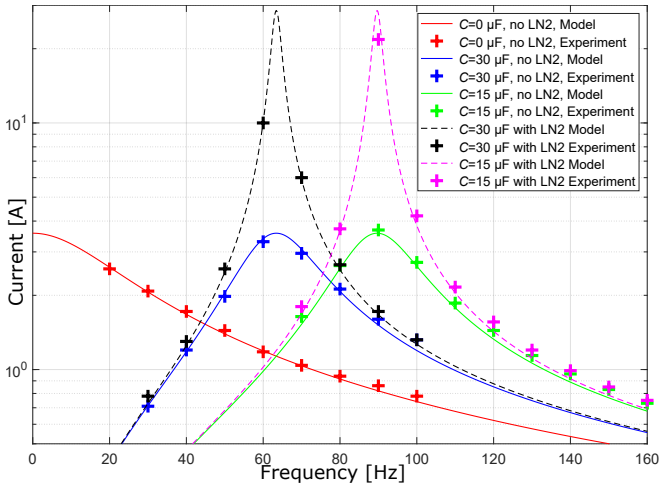

Fig. 5. Plot of the theoretical and experimental current inside an EM as a function of the frequency for a voltage of 100V. Values are expressed in terms of peak value. The average error between model and measurement is 3.97%.

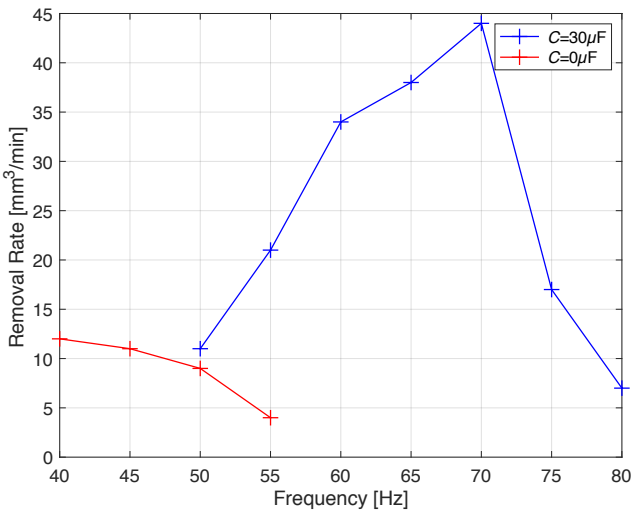

Fig. 6. Plot of the removal rate as a function of the frequency with and without capacitors in the circuit. Trials were run for no more than 10 minutes, and any trial that did not remove a clot within 10 minutes was recorded as a failure to remove the clot.

the swimmer rotates at the same frequency as the magnetic field. For $f_{\text{mf}} > f_{\text{so}}$ the swimmer can either stop rotating [17] or rotates at a speed lower than f_{mf} [39]. Fig. 6 shows that the removal with capacitors abruptly decreases at f=70Hz. This abrupt change in removal rates indicates that f_{so} was exceeded. The removal rate obtained without capacitors monotonically decreases between 40 and 45Hz. The removal rate obtained with capacitors is larger than without capacitors for frequencies greater or equal to 50Hz. The increased magnetic field at larger rotational frequencies enabled by the use of capacitors allow increasing the value of the removal rate by 266%. A maximum removal rate of 44mm^3/min was reached with capacitors, which is the highest values ever reported for a magnetic rotating swimmer.

IV. 3D PATH-FOLLOWING

A. Electric Model

This subsection presents the equations that link the currents and voltages across the EMs of a resonating magnetic manipulator having p EMs (p is the number of EMs). The total magnetic flux ϕ_t going through EM t is equal to the sum of the flux produced by this EM on itself and the flux produced by other EMs. It can be calculated using (1) where L_t is the self inductance of EM t, $M_{t,k}$ is the mutual inductance between EM t and EM k and I_k is the current that circulates in EM k:

$$\varphi_t = L_t \cdot I_t + \sum_{k=1}^{p,k\neq t} M_{t,k} \cdot I_k \tag{1}$$

This equation can be written for each EM and arranged into a matrix form:

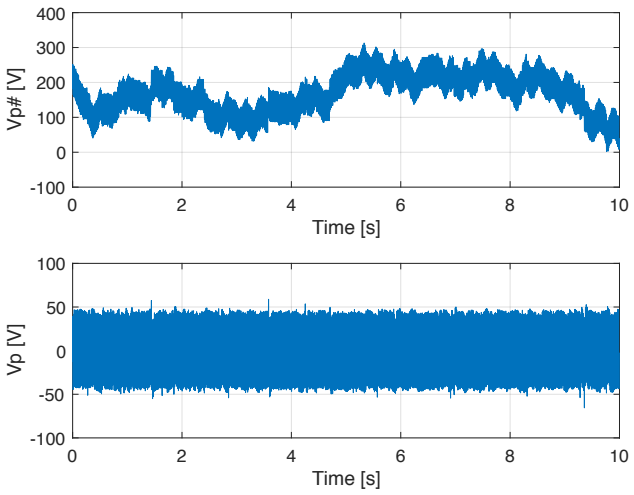

Fig. 7. Plot of voltage calculated by the EMSM before and after filtering.

$$\begin{bmatrix} \varphi_1 \\ \vdots \\ \varphi_k \\ \vdots \\ \varphi_p \end{bmatrix} = \begin{bmatrix} L_1 & \cdots & M_{1,k} & \cdots & M_{1,p} \\ \vdots & \ddots & & & \vdots \\ M_{k,1} & & L_k & & M_{k,p} \\ \vdots & & & \ddots & \vdots \\ M_{p,1} & \cdots & M_{p,k} & \cdots & L_p \end{bmatrix} \cdot \begin{bmatrix} I_1 \\ \vdots \\ I_k \\ \vdots \\ I_p \end{bmatrix},$$
$$\boldsymbol{\varphi} = \boldsymbol{L} \cdot \boldsymbol{i} \tag{2}$$

The voltage $\boldsymbol{v_l}$ induced on the EMs by the magnetic flux variation is:

$$\boldsymbol{v_l} = \frac{\mathrm{d}\boldsymbol{\varphi}}{\mathrm{d}t} = \boldsymbol{L} \cdot \frac{\mathrm{d}\boldsymbol{i}}{\mathrm{d}t} \tag{3}$$

The electric equation for the capacitors is:

$$\boldsymbol{i} = \boldsymbol{C} \cdot \frac{\mathrm{d}\boldsymbol{v_c}}{\mathrm{d}t} \text{ with } \boldsymbol{C} = \begin{bmatrix} C_1 & \cdots & 0 & \cdots & 0 \\ \vdots & \ddots & & & \vdots \\ 0 & & C_k & & 0 \\ \vdots & & & \ddots & \vdots \\ 0 & \cdots & 0 & \cdots & C_p \end{bmatrix} \quad (4)$$

The voltage produced created by the resistance of the EM is calculated via Ohm's law:

$$\boldsymbol{v_r} = \boldsymbol{R} \cdot \boldsymbol{i} \text{ with } \boldsymbol{R} = \begin{bmatrix} R_1 & \cdots & 0 & \cdots & 0 \\ \vdots & \ddots & & & \vdots \\ 0 & & R_k & & 0 \\ \vdots & & & \ddots & \vdots \\ 0 & \cdots & 0 & \cdots & R_p \end{bmatrix} \quad (5)$$

Equations 3, 4 and 5 can be combined to obtain the following differential equation:

$$\frac{\mathrm{d}\boldsymbol{v_p}}{\mathrm{d}t} = \boldsymbol{C}^{-1} \cdot \boldsymbol{i} + \boldsymbol{R} \cdot \frac{\mathrm{d}\boldsymbol{i}}{\mathrm{d}t} + \boldsymbol{L} \cdot \frac{\mathrm{d}^2\boldsymbol{i}}{\mathrm{d}^2t} \quad (6)$$

B. Equation solver

Equation 6 is solved in real-time to compute the voltage to apply to each EM. Equations 7 to 10 were implemented and computed at each program iteration. These equations were obtained by discretization of Equation 6 and by multiplying the result by δt. At each time step, the desired flux density is known as it is computed by the path controller (see IV-D). It is used as input for Equation 7 and allows the calculation of Equations 8 to 10.

$$\boldsymbol{\delta_{1i}}(t) = \boldsymbol{i}(t) - \boldsymbol{i}(t - \delta t) \quad (7)$$

$$\boldsymbol{\delta_{2i}}(t) = \boldsymbol{\delta_{1i}}(t) - \boldsymbol{\delta_{1i}}(t - \delta t) \quad (8)$$

$$\boldsymbol{\delta_{v_p}}(t) = \boldsymbol{C}^{-1} \cdot \boldsymbol{i}(t) \cdot \delta t + \boldsymbol{R} \cdot \boldsymbol{\delta_{1i}}(t) + \boldsymbol{L} \cdot \boldsymbol{\delta_{2i}}(t)/\delta t \quad (9)$$

$$\boldsymbol{v_p}(t) = \boldsymbol{v_p}(t-1) + \boldsymbol{\delta_{v_p}}(t) \quad (10)$$

C. Electromagnetic Model and Solver Module

Different methods are available to control the current inside a high power electric circuit. Current mode power supplies use a current sensor and a regulation loop to output the voltage value that will produce the desired current [40]. While sufficient for some applications, this solution does not take advantage of information about the system being driven. For example, the EMs of the system interact magnetically, and a current change in one EM induces a voltage in the others, which is not taken into account.

Fig. 8(a) presents the solution generally chosen for magnetic manipulation, using a current mode power supply. In this diagram, i_n^* is an element of $\boldsymbol{i^*}$, the current reference vector. Fig. 8(b) presents a new open-loop control solution that uses the new EMSM. The EMSM takes as input a vector $\boldsymbol{i^*}$ containing the current to apply to each EM. The current vector is first differentiated twice, and the values obtained are used in the Electric model presented in Section IV-A. The electric model predicts the variation of the voltage vector (voltage output needed on each power supply) which

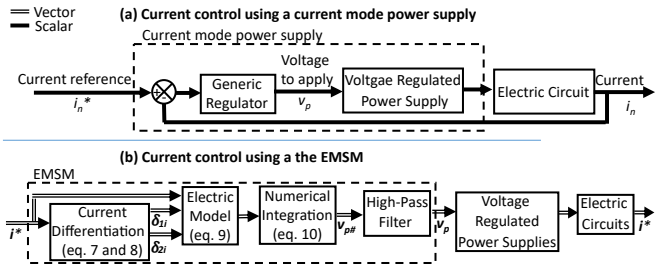

Fig. 8. Diagrams presenting different architectures of current controllers for magnetic manipulators.

is integrated to obtain the theoretical voltage to apply. This variable is the result of numerical integration of a type of operation that can lead to error accumulation and slowly drift. Fig. 7 (top) presents experimental values obtained from one element of $\boldsymbol{V_{p\#}}$ plotted as a function of time. It can be seen that the signal drifts and that the average value over a few rotations of the swimmer is not equal to zero. The power supplies cannot output the high average voltage value. A high pass filter was used to remove this average value (see Fig. 7 (bottom)) and calculate $\boldsymbol{V_p}$, the voltage value requested to the power supplies.

D. Path controller

The path controller used in the present study is based on the controller presented in [41] which was modified to accommodate the tested current controllers described in Section IV-C. It was also updated to take into account and compensate for the centripetal force.

The path controller takes as input the position $\boldsymbol{P}$ of the swimmer and the path data $\boldsymbol{T}$. Two Basler cameras are used together with a LabVIEW computer vision modules to calculate $\boldsymbol{P}$. The matrix $\boldsymbol{T}$ is manually defined and contains a set of points that belong to the path centerline. A path controller (see Fig. 9) first interpolates the path data to produce a high definition centerline to follow. The point of the path that is the closest to the swimmer is selected. The sum of the forces to apply to the swimmer is determined. This includes the weight, the drag, the centripetal force and an additional component calculated by a PID regulator to keep the swimmer on the centerline. The swimmer rotation vector $\boldsymbol{\omega}$ that produces the desired force is estimated using a first-order model. The desired magnetic flux density can be calculated because under the step-out frequency the field rotates at the same speed as the swimmer. The current to apply to the EMS is then calculated by using the inverse magnetic method described in [29].

E. Experiment results

The 3D path controller was implemented in LabVIEW. It was tested using the helical swimmer presented in Section II swimming inside the blood rheology mimicking solution (see Subsection II-B). Each EM was connected in series with a $30\mu F$ capacitor. The two current controllers described in Subsection IV-C were tested and the experimental paths

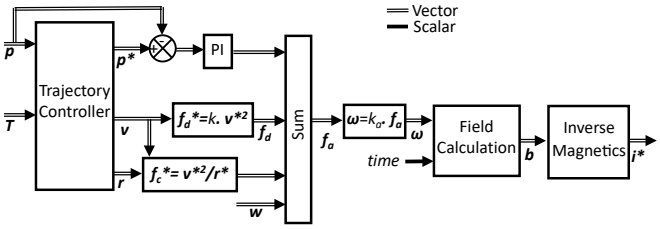

Fig. 9. Block diagram presenting the structure of the path controller.

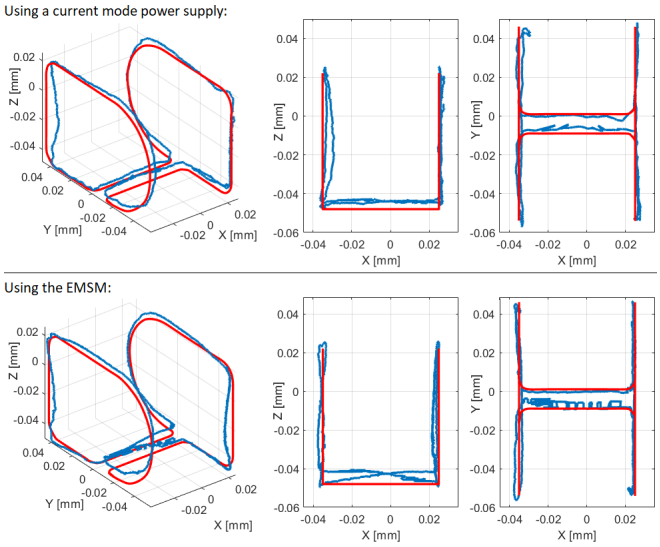

Fig. 10. Plot of the experimental paths followed by the swimmer (Red: Centerline, Blue: Experiment result). Top: Using a current mode power supply. Bottom: using the EMSM.

obtained are showed in Fig. 10. Both current control methods present similar performances. The average path tracking error is 3.4 and 3.1mm for the current mode power supplies and EMSM respectively. The EMSM allows 3D closed-loop path following without a current sensor which presents several advantages. The EMSM offers a solution for controlling the current of a resonating magnetic manipulator that is more robust against electromagnetic noise and is simpler to design, implement and operate.

V. Conclusion

This paper introduces a method for the 3D closed-loop control of a rotating magnetic swimmer using a resonating magnetic manipulator and a voltage mode power supply. This type of power supply is more straightforward, cheaper, and more common than current regulated power supplies. The manipulator system includes capacitors that compensate for the reactive power used by the EMs at the resonating frequency. A new EMSM that allows open-loop control of the current inside the EMs is presented and used experimentally. The experiment showed that the presented model enables the 3D control of the rotating swimmer using a resonating magnetic manipulator with a simple voltage mode power supply. Furthermore, the advantages of capacitors were highlighted, and the system was tested by removing a realistic blood clot model made with human blood. The addition of the capacitors allowed an increase of 266% of the removal rate. The maximum removal rate obtained, 44mm^3/min is the highest reported in the literature for this type of device when tested on a real blood clot. Previously reported values were equal to 20.13mm^3/min in [24], 1.43mm^3/min in [42], 0.614mm^3/min in [18], and 0.56mm^3/min in [19]. Our millimeter-scale swimmer is intended to be used inside the large arteries of the human body. It could, for example, be used to treat pulmonary embolism, and address limitations in current treatment options. A high removal rate will be paramount to the success of the procedure because blood clots in pulmonary arteries are large.

This study shows that the addition of capacitors to our laboratory magnetic manipulator increases the performance of the system in terms of maximum flux density and rotational speed. For the design of a clinical magnetic manipulator, the maximum flux density and rotational speed will be part of the design constraints. The use of capacitors will, in this case, decrease the power needed to produce the desired field. The power supplies are currently the most expensive component of our system. The addition of capacitors would enable the reduction of the cost of clinical manipulators by reducing the power rating of the power supplies and the electrical network needed.

References

[1] K. E. Peyer, S. Tottori, F. Qiu, L. Zhang, and B. J. Nelson, "Magnetic Helical Micromachines," *Chemistry - A European Journal*, vol. 19, no. 1, pp. 28–38, jan 2013. [Online]. Available: http://doi.wiley.com/10.1002/chem.201203364

[2] J. J. Abbott, K. E. Peyer, M. C. Lagomarsino, L. Zhang, L. Dong, I. K. Kaliakatsos, and B. J. Nelson, "How Should Microrobots Swim?" *The International Journal of Robotics Research*, vol. 28, no. 11-12, pp. 1434–1447, nov 2009. [Online]. Available: http://journals.sagepub.com/doi/10.1177/0278364909341658

[3] F. Ullrich, F. Qiu, J. Pokki, T. Huang, S. Pane, and B. J. Nelson, "Swimming characteristics of helical microrobots in fibrous environments," in *2016 6th IEEE International Conference on Biomedical Robotics and Biomechatronics (BioRob)*. IEEE, jun 2016, pp. 470–475. [Online]. Available: http://ieeexplore.ieee.org/document/7523671/

[4] T. Xu, G. Hwang, N. Andreff, and S. Regnier, "Modeling and Swimming Property Characterizations of Scaled-Up Helical Microswimmers," *IEEE/ASME Transactions on Mechatronics*, vol. 19, no. 3, pp. 1069–1079, jun 2014. [Online]. Available: http://ieeexplore.ieee.org/document/6553581/

[5] Huaming Li, Jindong Tan, and Mingjun Zhang, "Dynamics modeling and analysis of a swimming microrobot for controlled drug delivery," in *Proceedings 2006 IEEE International Conference on Robotics and Automation, 2006. ICRA 2006.* IEEE, 2006, pp. 1768–1773. [Online]. Available: http://ieeexplore.ieee.org/document/1641962/

[6] F. Z. Temel and S. Yesilyurt, "Magnetically actuated micro swimming of bio-inspired robots in mini channels," in *2011 IEEE International Conference on Mechatronics*. IEEE, apr 2011, pp. 342–347. [Online]. Available: http://ieeexplore.ieee.org/document/5971307/

[7] W. Gao, X. Feng, A. Pei, C. R. Kane, R. Tam, C. Hennessy, and J. Wang, "Bioinspired Helical Microswimmers Based on Vascular Plants," *Nano Letters*, vol. 14, no. 1, pp. 305–310, jan 2014. [Online]. Available: http://pubs.acs.org/doi/10.1021/nl404044d

[8] A. Ghosh and P. Fischer, "Controlled Propulsion of Artificial Magnetic Nanostructured Propellers," *Nano Letters*, vol. 9, no. 6, pp. 2243–2245, jun 2009. [Online]. Available: http://pubs.acs.org/doi/abs/10.1021/nl900186w

[9] A. W. Mahoney, J. C. Sarrazin, E. Bamberg, and J. J. Abbott, "Velocity control with gravity compensation for magnetic helical microswimmers," *Advanced Robotics*, vol. 25, no. 8, pp. 1007–1028, 2011.

[10] F. Z. Temel, A. E. Bezer, and S. Yesilyurt, "Navigation of mini swimmers in channel networks with magnetic fields," in *2013 IEEE International Conference on Robotics and Automation*. IEEE, may 2013, pp. 5335–5340. [Online]. Available: http://ieeexplore.ieee.org/document/6631341/

[11] T. Xu, G. Hwang, N. Andreff, and S. Regnier, "Characterization of three-dimensional steering for helical swimmers," in *2014 IEEE International Conference on Robotics and Automation (ICRA)*. IEEE, may 2014, pp. 4686–4691. [Online]. Available: http://ieeexplore.ieee.org/document/6907544/

[12] T. Xu, G. Hwang, N. Andreff, and S. Régnier, "Planar path following of 3-d steering scaled-up helical microswimmers," *IEEE Transactions on Robotics*, vol. 31, no. 1, pp. 117–127, Feb 2015.

[13] A. Hosney, A. Klingner, S. Misra, and I. S. M. Khalil, "Propulsion and steering of helical magnetic microrobots using two synchronized rotating dipole fields in three-dimensional space," in *2015 IEEE/RSJ International Conference on Intelligent Robots and Systems (IROS)*. IEEE, sep 2015, pp. 1988–1993. [Online]. Available: http://ieeexplore.ieee.org/document/7353639/

[14] K. Ishiyama, K. Arai, M. Sendoh, and A. Yamazaki, "Spiral-type micro-machine for medical applications," in *MHS2000. Proceedings of 2000 International Symposium on Micromechatronics and Human Science (Cat. No.00TH8530)*. IEEE, 2000, pp. 65–69. [Online]. Available: http://ieeexplore.ieee.org/document/903292/

[15] S. Lee, S. Lee, S. Kim, C.-H. Yoon, H.-J. Park, J.-y. Kim, and H. Choi, "Fabrication and characterization of a magnetic drilling actuator for navigation in a three-dimensional phantom vascular network," *Scientific reports*, vol. 8, no. 1, p. 3691, 2018.

[16] X. Wu, J. Liu, C. Huang, M. Su, and T. Xu, "3-d path following of helical microswimmers with an adaptive orientation compensation model," *IEEE Transactions on Automation Science and Engineering*, 2019.

[17] J. Leclerc, H. Zhao, D. Z. Bao, A. T. Becker, M. Ghosn, and D. J. Shah, "Agile 3d-navigation of a helical magnetic swimmer," in *Robotics and Automation (ICRA), 2020 IEEE International Conference on*. IEEE, 2020.

[18] I. S. Khalil, D. Mahdy, A. El Sharkawy, R. R. Moustafa, A. F. Tabak, M. E. Mitwally, S. Hesham, N. Hamdi, A. Klingner, A. Mohamed *et al.*, "Mechanical rubbing of blood clots using helical robots under ultrasound guidance," *IEEE Robotics and Automation Letters*, vol. 3, no. 2, pp. 1112–1119, 2018.

[19] I. S. Khalil, A. F. Tabak, K. Sadek, D. Mahdy, N. Hamdi, and M. Sitti, "Rubbing against blood clots using helical robots: modeling and in vitro experimental validation," *IEEE Robotics and Automation Letters*, vol. 2, no. 2, pp. 927–934, 2017.

[20] D. Mahdy, N. Hamdi, S. Hesham, A. El Sharkawy, and I. S. Khalil, "The influence of mechanical rubbing on the dissolution of blood clots," in *2018 40th Annual International Conference of the IEEE Engineering in Medicine and Biology Society (EMBC)*. IEEE, 2018, pp. 1660–1663.

[21] Q. Pan, S. Guo, and T. Okada, "Mechanism and control of a spiral type microrobot," in *The 2010 IEEE International Conference on Information and Automation*. IEEE, jun 2010, pp. 735–740. [Online]. Available: http://ieeexplore.ieee.org/document/5512476/

[22] W. Lee, S. Jeon, J. Nam, and G. Jang, "Dual-body magnetic helical robot for drilling and cargo delivery in human blood vessels," *Journal of Applied Physics*, vol. 117, no. 17, p. 17B314, may 2015. [Online]. Available: http://aip.scitation.org/doi/10.1063/1.4917067

[23] A. Oulmas, N. Andreff, and S. Régnier, "3d closed-loop swimming at low reynolds numbers," *The International Journal of Robotics Research*, vol. 37, no. 11, pp. 1359–1375, 2018.

[24] J. Leclerc, H. Zhao, D. Bao, and A. T. Becker, "In vitro design investigation of a rotating helical magnetic swimmer for combined 3-d navigation and blood clot removal," *IEEE Transactions on Robotics*, vol. 36, no. 3, pp. 975–982, 2020.

[25] V. F. Tapson, "Acute pulmonary embolism," *New England Journal of Medicine*, vol. 358, no. 10, pp. 1037–1052, 2008.

[26] M. V. Huisman, S. Barco, S. C. Cannegieter, G. Le Gal, S. V. Konstantinides, P. H. Reitsma, M. Rodger, A. V. Noordegraaf, and F. A. Klok, "Pulmonary embolism," *Nature Reviews Disease Primers*, vol. 4, no. 1, p. 18028, 2018. [Online]. Available: https://doi.org/10.1038/nrdp.2018.28

[27] I. Kürkciyan, G. Meron, F. Sterz, K. Janata, H. Domanovits, M. Holzer, A. Berzlanovich, H. C. Bankl, and A. N. Laggner, "Pulmonary embolism as cause of cardiac arrest: presentation and outcome," *Archives of internal medicine*, vol. 160, no. 10, pp. 1529–1535, 2000.

[28] M. Leacche, D. Unic, S. Z. Goldhaber, J. D. Rawn, S. F. Aranki, G. S. Couper, T. Mihaljevic, R. J. Rizzo, L. H. Cohn, L. Aklog *et al.*, "Modern surgical treatment of massive pulmonary embolism: results in 47 consecutive patients after rapid diagnosis and aggressive surgical approach," *The Journal of Thoracic and Cardiovascular Surgery*, vol. 129, no. 5, pp. 1018–1023, 2005.

[29] J. Leclerc, B. Isichei, and A. T. Becker, "A magnetic manipulator cooled with liquid nitrogen," *IEEE Robotics and Automation Letters*, vol. 3, no. 4, pp. 4367–4374, 2018.

[30] C. Kearon, "Natural history of venous thromboembolism," *Circulation*, vol. 107, no. 23_suppl_1, pp. I–22, 2003.

[31] M. G. Davies and H. F. El-Sayed, "Current status of clot removal for acute pulmonary embolism," *Annals of vascular surgery*, vol. 31, pp. 211–220, 2016.

[32] J. Llevadot, R. P. Giugliano, and E. M. Antman, "Bolus fibrinolytic therapy in acute myocardial infarction," *Jama*, vol. 286, no. 4, pp. 442–449, 2001.

[33] M. S. Makary, B. D. Fogler, P. P. Dube, V. L. Flanders, K. Natarajan, R. Garcia-Cortes, T. Foster, and J. D. Dowell, "Ultrasound-accelerated, catheter-directed thrombolysis for submassive pulmonary embolism: Single-center retrospective review with intermediate-term outcomes," *Journal of Vascular and Interventional Radiology*, vol. 31, no. 3, pp. 438–443, 2020.

[34] I. Papanicolas, L. R. Woskie, and A. K. Jha, "Health Care Spending in the United States and Other High-Income Countries," *JAMA*, vol. 319, no. 10, pp. 1024–1039, 03 2018. [Online]. Available: https://doi.org/10.1001/jama.2018.1150

[35] J. Nam, W. Lee, B. Jang, and G. Jang, "Magnetic navigation system utilizing resonant effect to enhance magnetic field applied to magnetic robots," *IEEE Transactions on Industrial Electronics*, vol. 64, no. 6, pp. 4701–4709, 2017.

[36] R. Mammano, "Switching power supply topology voltage mode vs. current mode," *Elektron Journal-South African Institute of Electrical Engineers*, vol. 18, no. 6, pp. 25–27, 2001.

[37] R. S. Rosenson, A. Mccormick, and E. F. Uretz, "Distribution of blood viscosity values and biochemical correlates in healthy adults." *Clinical Chemistry*, vol. 42, no. 8, pp. 1189–1195, 1996.

[38] H. Hinghofer-Szalkay and J. Greenleaf, "Continuous monitoring of blood volume changes in humans," *Journal of applied physiology*, vol. 63, no. 3, pp. 1003–1007, 1987.

[39] A. W. Mahoney, N. D. Nelson, K. E. Peyer, B. J. Nelson, and J. J. Abbott, "Behavior of rotating magnetic microrobots above the step-out frequency with application to control of multi-microrobot systems," *Applied Physics Letters*, vol. 104, no. 14, p. 144101, apr 2014. [Online]. Available: http://aip.scitation.org/doi/10.1063/1.4870768

[40] L. Dixon, "Average current mode control of switching power supplies," in *Unitrode Power Supply Design Seminar Handbook*. Unitrode Corporation, 1990, pp. 5–1.

[41] J. Leclerc, H. Zhao, and A. T. Becker, "3d control of rotating millimeter-scale swimmers through obstacles," in *2019 International Conference on Robotics and Automation (ICRA)*. IEEE, 2019, pp. 8890–8896.

[42] I. S. Khalil, A. Adel, D. Mahdy, M. M. Micheal, M. Mansour, N. Hamdi, and S. Misra, "Magnetic localization and control of helical robots for clearing superficial blood clots," *APL bioengineering*, vol. 3, no. 2, p. 026104, 2019.